# Automatic Uncertainty-Aware Synthetic Data Bootstrapping for Historical Map Segmentation

Lukas Arzoumanidis<sup>1\*</sup>, Julius Knechtel<sup>2</sup>, Jan-Henrik Haunert<sup>2</sup>, Youness Dehbi<sup>1</sup>

 <sup>1\*</sup>Computational Methods Lab, HafenCity University, Henning-Voscherau-Platz 1, Hamburg, 20457, Germany.
 <sup>2</sup>Institute of Geodesy and Geoinformation, University of Bonn, Meckenheimer Allee 172, Bonn, 53115, North Rhine-Westphalia, Germany.

\*Corresponding author(s). E-mail(s): lukas.arzoumanidis@hcu-hamburg.de; Contributing authors: knechtel@igg.uni-bonn.de; haunert@igg.uni-bonn.de; youness.dehbi@hcu-hamburg.de;

#### Abstract

The automated analysis of historical documents, particularly maps, has drastically benefited from advances in deep learning and its success across various computer vision applications. However, most deep learning-based methods heavily rely on large amounts of annotated training data, which are typically unavailable for historical maps, especially for those belonging to specific, homogeneous cartographic domains, also known as corpora. Creating high-quality training data suitable for machine learning often takes a significant amount of time and involves extensive manual effort. While synthetic training data can alleviate the scarcity of real-world samples, it often lacks the affinity (realism) and diversity (variation) necessary for effective learning. By transferring the cartographic style of an original historical map corpus onto vector data, we bootstrap an effectively unlimited number of synthetic historical maps suitable for tasks such as land-cover interpretation of a homogeneous historical map corpus. We propose an automatic deep generative approach and a alternative manual stochastic degradation technique to emulate the visual uncertainty and noise, also known as data-dependent uncertainty, commonly observed in historical map scans. To quantitatively evaluate the effectiveness and applicability of our approach, the generated training datasets were employed for domain-adaptive semantic segmentation on a homogeneous map corpus using a Self-Constructing Graph Convolutional Network, enabling a comprehensive assessment of the impact of our data bootstrapping methods.

**Keywords:** training data generation, aleatoric uncertainty simulation, cartographic style transfer, historical maps, domain-adaptive semantic segmentation

#### 1 Introduction

Historical maps constitute an essential resource for the reconstruction and monitoring of environmental and spatio-temporal changes, representing a fundamental source of geographic information [1]. They provide a detailed depiction of the spatial configuration of the Earth's surface over extended temporal intervals preceding the advent of modern Earth observation technologies. To ensure long-term preservation and accessibility, historical maps are typically digitized and stored as raster images in archival databases. However, this process strips away their inherent semantic content, rendering the underlying spatio-temporal knowledge inaccessible to computational analysis. Consequently, to extract this embedded information in a machine-readable and processable form, historical maps must first undergo semantic interpretation. For many decades, the extraction of semantic information from historical maps was

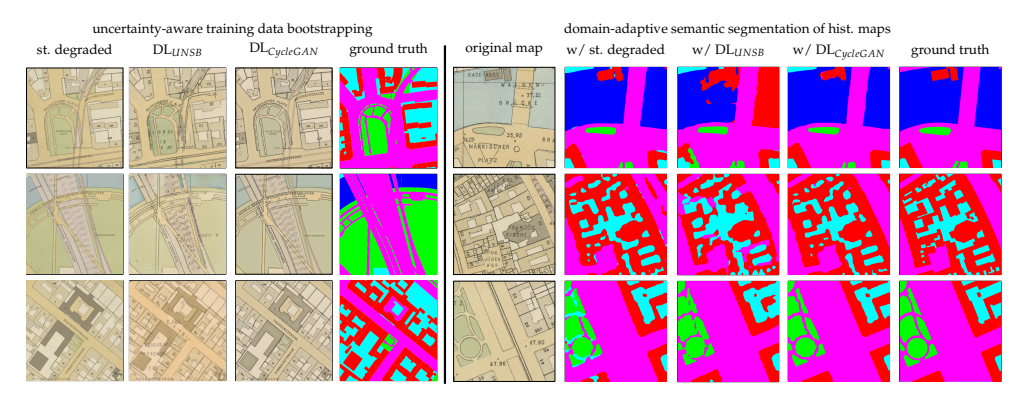


Fig. 1: Generated synthetic historical maps (left) and results of semantic segmentation of original historical maps (right).

conducted manually or through semi-automated workflows – processes that were both time-consuming and labor-intensive [1]. In recent years, deep neural networks have gained significant traction and demonstrated state-of-the-art performance across numerous tasks related to the automatic analysis of historical maps, including object extraction [2, 3] and semantic segmentation [4, 5]. Such advancements have facilitated progress in multiple research areas, including road extraction [6–8], urbanization studies [9], and land-use change detection [10, 11]. Despite these successes, deep learning-based approaches for supervised tasks, such as semantic segmentation,

demand substantial quantities of pre-annotated high quality training data – resources that remain extremely limited for historical maps, especially for single map types or periods [1, 12]. As a result, existing methodologies either rely heavily on manually annotated datasets which is a costly and labor-intensive process that contradicts the very goal of automation or employ transfer learning techniques, such as domain adaptation [13], by utilizing data from other visual domains. More recently, several emerging approaches have sought to overcome the limitations associated with data scarcity and domain heterogeneity. These include the use of visual foundation models [14, 15], Large Language Models (LLMs) [16, 17], synthetic data generation for domain-specific training [10, 17], and transformer-based architectures for robust and scalable map interpretation [4, 7]. Nevertheless, these approaches often encounter challenges related to domain mismatch and limited generalization, primarily caused by the stylistic heterogeneity of historical map corpora. Such variability arises from differences in typeface, symbology, color palette, and scale [5], as well as from datadependent uncertainty, also referred to as aleatoric uncertainty, introduced by map degradation effects such as color fading, folding marks, dust accumulation, or mildew stains.

A commonly adopted strategy to overcome the scarcity of annotated data is the automatic generation of synthetic training datasets through simulation. In various domains such as autonomous driving and precision agriculture, synthetic data have been successfully employed for tasks including classification [18], object detection [2], and semantic segmentation [19]. Simulated datasets can capture a significant portion of the data-dependent uncertainty inherent to real-world distributions, enabling the creation of large-scale, domain-representative training corpora. This capability renders data-intensive machine learning methods both feasible and effective. Despite its success in other fields, the use of simulation for synthetic data generation in the context of historical maps remains limited. Existing efforts have primarily focused on specific applications such as automated text detection [2, 20], road extraction [8] or for the analysis of land use and land-cover change [10].

We propose a novel and highly effective approach for synthesizing historical maps within homogeneous cartographic corpora by employing Generative Adversarial Networks (GANs) and Stable Diffusion (SD) – and benchmarking their performance against stochastic degradation-based image augmentation techniques. Our approach provides explicit control over spatial layouts through a semantically guided, unpaired image-to-image style transfer framework. We validate the effectiveness and practical applicability of our approach by manually annotating historical maps from a homogeneous urban map corpus and performing domain-adaptive semantic segmentation using a model trained exclusively on the bootstrapped historical maps to extract land-use information. Explicit control over the spatial layout of semantic vector data is achieved by synthesizing modern, arbitrary vector inputs in historical cartographic styles, enabling the generation of an unlimited amount of training data. In this work, we use the term bootstrapping to describe the automatic generation of synthetic training data for historical maps from existing spatial vector data, without

relying on paired training data or manually annotated map examples. To evaluate the practical utility of the proposed synthetic data, we trained a state-of-the-art graph-based deep learning model for semantic segmentation. The model, trained exclusively on data bootstrapped by our framework, was subsequently applied to the interpretation of an original historical map corpus. To further demonstrate the usability and potential applications of our approach, we developed an interactive web application that showcases its functionality for spatial analyses, such as urban change detection. The source code associated with this work is publicly available at <a href="https://github.com/hcu-cml/bootstrap-HistoricalMap">https://github.com/hcu-cml/bootstrap-HistoricalMap</a>.

The main contributions of this work are summarized as follows:

- We transfer the cartographic style of a homogeneous historical map corpus onto arbitrary vector data, while simulating aleatoric uncertainty to generate *unlimited* annotated training data for a specific homogeneous corpus,
- we evaluate the suitability of our synthetic training data by the Fréchet Inception
  Distance (FID) and through training a semantic segmentation model with it and
  applying the model on a historical map corpus,
- we significantly reduce the time required for manually annotating training data, cutting the process of interpreting land-cover classes from historical maps down to just a few hours.

The remainder of this paper is organized as follows: Section 2 reviews recent advances in the synthetic generation of historical maps. Section 3 describes the geospatial vector data and the original historical map corpus used in this study. Section 4 presents our proposed methodology in detail. Section 5 evaluates the quality of the generated training data and demonstrates the effectiveness of our semantic segmentation approach on historical maps. Finally, Section 6 concludes the paper and outlines directions for future research.

## 2 Related Work

Deep learning-based methodologies for the extraction of road networks from historical maps typically require extensive annotated training datasets. To address the scarcity of such data, Jiao et al. [8], Mühlematter et al. [21] introduced a simulation-based framework for road extraction and classification. Their method synthesizes training data by augmenting existing road geometries onto historical map backgrounds from the same cartographic corpus. While this strategy effectively expands the amount of available training data, it relies on the assumption that the vector data precisely correspond to the spatial layout of the historical map. In practice, however, this condition rarely holds, as the geometry and topology of road networks often evolve substantially over time. Moreover, the approach requires both the vector and raster datasets to be georeferenced, constraints that are not imposed by our proposed method.

In a related line of research, Affolter et al. [22] investigated the generation of historical maps with explicit spatial layout control by leveraging Stable Diffusion in combination with ControlNet [23]. Similar to the approaches proposed by Jiao et al.

[8], Mühlematter et al. [21], their method synthesizes historical maps using historical road network vector data as structural input. This form of map bootstrapping has precedents in other domains, such as the creation of two-dimensional figure—ground maps [24]. However, the approach by Affolter et al. [22] exhibits certain limitations. Most notably, it depends on the availability of georeferenced historical maps for training and employs a paired image—generation pipeline that integrates ControlNet conditioning with exact historical road network geometries. Such detailed and spatially aligned vector data are rarely available for historical periods, thereby introducing a dependency on pre-existing map interpretations and restricting the applicability of the method to well-documented regions or time frames. In contrast, we propose an approach that is entirely independent of paired training data for the bootstrapping of historical maps by transferring the cartographic style of an original historical map corpus onto vector data.

Recently, López-Rauhut et al. [10] introduced a dataset of historical maps designed to support the analysis of large-scale, long-term land-use and land-cover dynamics under limited annotation conditions. The dataset is used to conduct semantic segmentation of land-cover classes with both fully supervised and weakly supervised deep learning models trained on historical labels as well as modern annotations. In the weakly supervised setting, historical maps are first translated into a modern cartographic style using CycleGAN to reduce stylistic discrepancies, thereby enabling segmentation based on existing modern ground-truth labels. In contrast, we propose a domain-adaptive semantic segmentation approach that transfers the cartographic style of historical maps onto modern vector data, rather than translating historical maps into a modern style as in their work. Furthermore, we aim to reduce stylistic discrepancies in our bootstrapped historical maps by artificially degrading them with data-dependent noise.

To advance the automated interpretation of historical maps beyond geometrical feature extraction, the ability to read and understand textual map elements is of increasing importance. Textual labels provide valuable semantic information that supports both map interpretation and metadata enrichment. However, most existing approaches are trained on datasets from unrelated visual domains, resulting in limited generalization to historical cartographic materials. To mitigate this issue, Li et al. [2] proposed a synthetic data generation framework based on cartographic style transfer using Generative Adversarial Networks (GANs). Their model produces synthetic maps in which the placement, typography, and content of text labels can be fully controlled, enabling the creation of large-scale annotated datasets for training text recognition models. Extending this concept, Arzoumanidis et al. [12] developed a generative framework that learns the stylistic characteristics of diverse historical map corpora and applies them to contemporary urban maps, thereby producing a virtually unlimited number of synthetic historical maps. Building upon these prior works, our approach directly transfers the learned cartographic style of a historical map corpus onto arbitrary vector data, generating an effectively unlimited set of synthetic maps with perfectly aligned ground-truth annotations. To the best of our knowledge, such

direct coupling between vector-based content and learned cartographic style has not been previously investigated.

Complementary to data simulation strategies, several studies have focused on improving model performance under conditions of limited annotated data. Recent research has explored learning paradigms that enhance data efficiency in semantic segmentation and object detection tasks. These include spatio-temporal learning techniques that exploit temporal continuity to reduce annotation requirements [4, 25], domain adaptation frameworks that enable the transfer of learned representations across heterogeneous map collections [13], and unsupervised or self-supervised learning approaches that minimize reliance on labeled samples [14, 26].

Another emerging direction leverages the power of pre-trained foundation models and large multimodal networks for cartographic analysis [14, 26]. For instance, Yuan et al. [27] and Sterzinger et al. [15] demonstrated that few-shot segmentation models can be effectively adapted to historical maps, while Yuan and Sester [16] and Wang et al. [28] explored the integration of LLMs to support multimodal reasoning and semantic labeling. Collectively, these approaches highlight a paradigm shift from data-intensive learning toward methods that exploit prior knowledge, transfer learning, and generative modeling to mitigate data scarcity in the analysis of historical maps.

# 3 Map Corpus & Vector Data

The map corpus exemplarily worked with in this study comprises 39 historical urban maps of Berlin, Germany, provided by the State Library of Berlin, and represents five distinct land-cover classes, namely:

- 1. **Buildings** including public, private, military, and religious structures;
- 2. **Infrastructure** such as bridges, tunnels, streets, and railway tracks;
- 3. Recreational surfaces including parks, gardens, and cemeteries;
- 4. **Sealed surfaces** such as arterial roads, squares and backyards;
- 5. Water bodies comprising rivers, ponds, and fountains.

The maps share a common scale of 1:4000 and a consistent cartographic style, which allows the map corpus to be characterized as homogeneous. Since the primary objective of this work is the semantic segmentation of land-cover classes, we disregard the map frame entirely and focus exclusively on the map content itself. The modern vector data used in this study were primarily sourced from OpenStreetMap (OSM) [29]. This dataset provides detailed, real-world geometries for building footprints, land parcels, and street networks, making it well suited for cartographic reproduction. To achieve a more faithful replication, this foundational data were enriched with semantic information from Germany's Authoritative Cadastral Information System.

#### 4 Methods

In this section, we describe how geospatial vector data can be utilized to generate an *unlimited* number of training samples for domain-adaptive semantic segmentation of historical maps by explicitly controlling both the spatial composition and the semantic layout of the synthesized maps. The proposed workflow comprises four main components. First, we present our method for generating realistic synthetic historical maps that replicate the cartographic style of a specific homogeneous map corpus. We also describe how the corresponding land-cover annotations are derived to produce paired training samples required for deep learning-based semantic segmentation (cf. Figure 2). Second, we detail our approach for simulating data-dependent uncertainty by augmenting the style-transferred vector data with degradation effects derived from deep generative models or, alternatively, from manual stochastic degradation techniques (cf. Figure 2). To automatically degrade the bootstrapped training data with simulated data-dependent uncertainty, we employ two different deep learning-based generative approaches, namely, Generative Adversarial Networks (GANs) and Stable Diffusion (SD), for unpaired image-to-image translation. Finally, we demonstrate how the resulting synthetic data are employed within a graph-based deep learning framework to perform domain-adaptive semantic segmentation on previously unseen historical maps, and how the outcomes can be visualized and explored through an interactive web-based viewer (cf. Figure 2). More formally, our goal is to

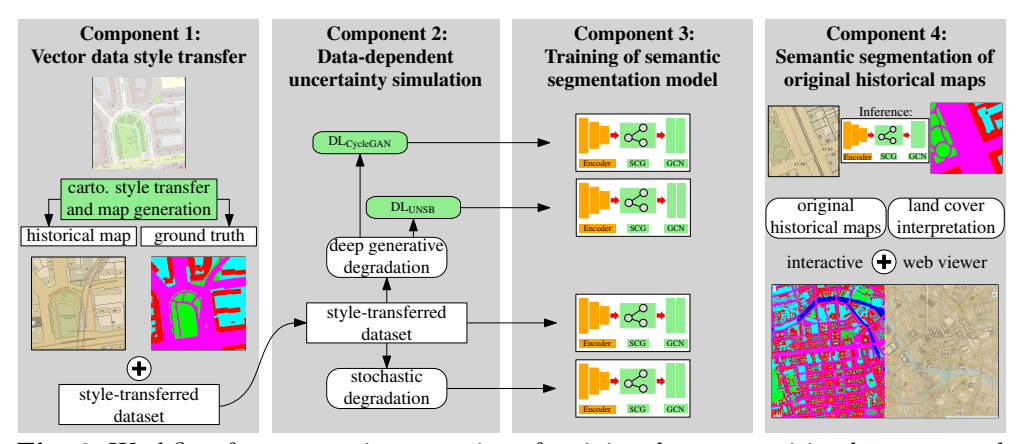


Fig. 2: Workflow for automatic generation of training data, comprising bootstrapped historical maps and their corresponding bootstrapped land-cover class annotations.

learn a mapping  $G: X \to Y$  such that the translation G(x) of any generated map  $x \in X$  simulates the data-dependent uncertainty within a historical map corpus Y, while preserving the cartographic style and semantic content, such as the spatial layout of the vector data underlying x.

Data-dependent uncertainty arising from the physical deterioration of original map sheets, archival storage conditions, or suboptimal scanning processes further complicates the generation of suitable training data for deep learning-based approaches. To ensure realistic learning behavior, the training data must accurately represent these inherent uncertainties across the entire data distribution. Typical degradation effects include paper distortion, folding marks, and additional impurities or artifacts such as dirt, dust, mildew stains, and color fading, as illustrated in Figure 3.



**Fig. 3**: Complications in the preservation of historical maps. Accumulation of dust and mildew stains as well as imprecisions in shading and coloring.

#### 4.1 Vector data style transfer

To manually replicate historical maps, the cartographic style of the original historical map is applied as accurately as possible to the vector data. To mitigate the influence of impurities, color fading, and compression artifacts when estimating the color code for each map object class, we computed the mean RGB value within a  $5\times5$  kernel. The estimation of stylistic elements, such as object coloration, line thicknesses of building footprints, street and parcel boundaries, as well as font types and sizes, is performed through limited manual effort based on visual inspection. Since the OSM vector data are already semantically categorized, the color representation of individual classes can be readily adjusted using visualization tools such as the maptiler [30] or maputnik [31], as demonstrated in our interactive web-based viewer<sup>1</sup>. In addition to the aforementioned elements, a coordinate grid was overlaid onto the vector data to replicate the layout conventions observed in the historical map corpus used in this study. The total time required to reproduce the cartographic style of a historical map corpus, such as the Staube maps, is less than two hours. To enrich the historical maps with house numbers within building footprints, street names aligned with their corresponding street geometries, and the names of cultural, historical, medical, and public institutions, as well as notable places, monuments, and landmarks, we utilize the semantic information derived from the OSM data. To bootstrap image pairs consisting of a generated map and its corresponding land-cover class annotations, the vector data were duplicated and aggregated according to the land-cover classes defined in Section 3. Notably, our approach allows users to specify custom patch dimensions, enabling the generation of training samples tailored to all kinds of homogeneous cartographic domains of varying and irregular formats. An example image pair, consisting of a synthetic historical map and its corresponding land-cover annotations bootstrapped via vector-based cartographic style transfer is shown in Figure 4. The training data bootstrapped through this process are referred to as the style-transfer dataset, as illustrated in Figure 2.

<sup>&</sup>lt;sup>1</sup>http://88.198.55.211/map/



**Fig. 4**: Bootstrapped map pair example comprising a synthetically generated historical map and simulated data-dependent uncertainty.

## 4.2 Data-dependent uncertainty simulation

By simulating data-dependent uncertainty to enhance the realism of our generated historical maps and provide a more robust foundation for domain-adaptive semantic segmentation, we introduce a stochastic degradation process applied to the purely style-transferred dataset, as illustrated in Figure 2. Since historical maps often exhibit visually complex and noisy backgrounds caused by imperfections introduced during their preservation, the generated historical maps were degraded to more faithfully replicate the cartographic style, including its inherent uncertainties, of the original map corpus by simulating data-dependent uncertainty. Although such uncertainty cannot be effectively modeled directly [4, 32], we instead simulate data-dependent uncertainty within the generated historical maps themselves.

Stochastic degradation. To this end, we first apply a Gaussian filter with a kernel size of  $3 \times 3$  to the bootstrapped training dataset. This operation smooths sharp edges and enhances visual realism, thereby approximating the data-dependent uncertainty typically observed after scanning historical maps. In addition, we introduce further uncertainty by randomly cropping, rotating, and overlaying a semi-transparent image of black dust<sup>2</sup> onto the training data. This step is intended to mimic common visual artifacts found in historical maps, such as dust accumulation and mildew stains. An example image pair comprising a synthetic historical map degraded through manual simulation of such data-dependent uncertainty is shown in Figure 4b. Consequently, we bootstrap a second synthetically generated training dataset, referred to as **stochastically** (st.) degraded, which incorporates minimal manual effort to improve the purely style-transferred dataset through the simulation of datadependent uncertainty, as illustrated in Figure 2. Furthermore, when rendering the purely style-transferred historical maps in vector format, anti-aliasing is enabled to reduce visual artifacts and eliminate the jagged appearance, thereby enhancing the overall visual quality of the maps.

Deep generative degradation. To further advance our approach and explore

 $<sup>^2 \</sup>rm https://pngtree.com/freepng/dust-overlay-element-png\_8071784.html$ 

methods for enhancing bootstrapped historical maps without manual intervention, we propose the use of deep generative models. Unlike our stochastical degradation method that relies on manual finetuning, these models are supposed to learn the datadependent uncertainty directly from the underlying data enabling fully automated degradation. We selected the cycle-consistent adversarial network CycleGAN [33] for our GAN-based experiments because it is widely recognized for achieving competitive results in image generation across diverse scientific domains and, more importantly, has already been successfully applied to the cartographic domain [2, 12]. For our second deep generative approach, we selected Stable Diffusion (SD), as it has recently demonstrated promising results for the generation of historical maps [22]. Specifically, we utilized Unpaired Neural Schrödinger Bridge (UNSB), which has recently been successfully applied to unpaired image-to-image translation tasks and style transfer in complex visual domains [34]. As a result, we produce a third and forth bootstrapped training dataset, as illustrated in Figure 2. To facilitate the distinction between each dataset and its corresponding model, we introduce  $DL_{CycleGAN}$  dataset and **DL**<sub>UNSB</sub> dataset, which represent the incorporation of deep learning-based, datadependent uncertainty simulation, as illustrated in Figure 4c.

The CycleGAN model learns to translate the style from the input domain Y to the input domain X in an unpaired manner, using an architecture composed of two image Generators, G and F, and two image Discriminators,  $D_x$  and  $D_y$  as illustrated in Figure 5a. The architecture of an image Generator is composed of convolutional layers that encode latent features into a higher-dimensional space by progressively increasing the number of image channels. In our implementation, the original CycleGAN architecture was adapted to process input images with dimensions of  $500 \times 500 \times 3$ . Residual blocks are then applied to preserve high-quality image details while maintaining style consistency and semantic fidelity. Finally, a decoder upsamples the high-dimensional feature representation back to the original image resolution of  $500 \times 500 \times 3$  [33]. The Discriminator architecture is based on a PatchGAN module, which evaluates whether an input image is real or generated. To ensure generative realism in the synthesized historical maps and to enforce cycle-consistency, i.e., the ability to transform handcrafted maps into historical-style maps and reconstruct them back, CycleGAN employs two distinct loss functions, each serving a specific purpose. The adversarial loss incentivizes the Generator to produce outputs that are indistinguishable from real images Y within the target domain X. To prevent arbitrary permutations of images within the target domain, a cycle-consistency loss is introduced. This loss constrains the space of possible mapping functions by enforcing that, for each image x from domain X, the translation cycle should be capable of reconstructing the original image [33]. In our setup, set X corresponds to the bootstrapped historical maps, while set Y comprises maps from an original, homogeneous corpus. Generator G translates maps from domain X into the style of domain Y, producing Y. This translated map is then passed through Generator F, which reconstructs it back into domain X, yielding  $\hat{X}$ . In the second cycle, maps from set Y are translated into domain X using Generator F, resulting in  $\hat{X}$ , which are subsequently translated back to domain Y using Generator G, producing  $\hat{Y}$ . This cycle-consistency

process is illustrated in Figure 5b.

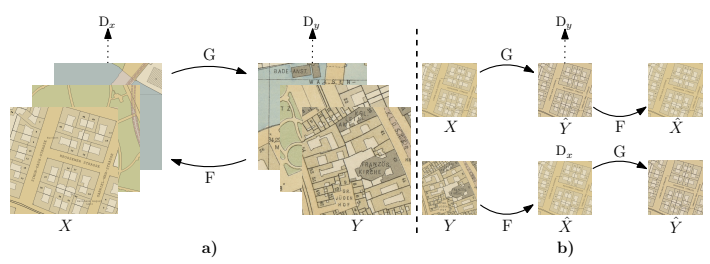


**Fig. 5**: Generator-Discriminator interplay of the underlying CycleGAN for data-dependent uncertainty simulation in style-transferred historical maps.

For generating visually realistic historical maps with simulated data-dependent uncertainty, we evaluate an early training epoch, selected before the onset of noticeable changes in map geometry or object topology. We found that this approach effectively captures early-stage cartographic style refinements and data-dependent uncertainty while avoiding later-stage translations that could compromise control over the spatial layout of the semantic vector data. To validate early-stage checkpoints, we assess the generated map tiles through **Fréchet Inception Distance (FID)** scores [35]. This ensures that the synthetic training data remains both stylistically consistent and topologically faithful to the original annotations used as ground truth.

The Unpaired Neural Schrödinger Bridge (UNSB) model formulates unpaired imageto-image translation as a discretised Schrödinger Bridge (SB) problem. Within the SB framework, the objective is to identify the most probable stochastic process  $(X_t)_{t\in[0,1]}$  that transports a source distribution  $p_0$ , representing the cartographic style of historical maps, to a target distribution  $p_1$ , corresponding to the style-transferred vector data, while maintaining proximity to a prescribed reference diffusion process q. This can be expressed as minimising the Kullback-Leibler divergence.

Because solving this optimisation directly is infeasible for high-dimensional images, the Unpaired Neural Schrödinger Bridge (UNSB) approximates the continuous-time solution through a series of discrete steps  $X_{t_{k+1}} = G_{\theta_k}(X_{t_k})$ , where each generator  $G_{\theta_k}$  performs a small, incremental transformation. Instead of learning a single complex mapping, the model constructs a chain of simpler transitions that, together, approximate the SB path from the cartographic appearance of the original historical maps, including its data-depended uncertainty, to the style-transferred vector data. To guide this progression, UNSB employs a time-conditioned Discriminator that assesses whether intermediate samples resemble the corresponding stage of the target distribution. Although adversarial losses are used, each step essentially receives feedback on how closely its outputs match the cartographic characteristics of the style-transferred vector data, without requiring explicit likelihood modelling. To pre-

serve geographic structure, UNSB incorporates lightweight identity and consistency

regularisers that encourage  $G_{\theta_k}(x) \approx x$  for inputs that should maintain their spatial form, similar to the cycle-consistency loss that enforces the ability to map a generated historical map forward and then back to its original form in CycleGAN [34]. These constraints help prevent distortions of map geometry, such as boundaries, networks, or contours, ensuring that stylistic translation does not compromise the semantic information required for downstream segmentation tasks.

While CycleGAN also enables unpaired image-to-image translation, its mechanism differs fundamentally from the UNSB framework. CycleGAN learns two deterministic mappings between domains, constrained by a cycle-consistency loss that enforces the ability to map an image forward and then back to its original form. Although this promotes content preservation, it does not provide a principled way to model the distributional evolution between domains. In contrast, UNSB constructs a stochastic transport path between the cartographic style and data-dependend uncertainty of the original historical maps and cartographic appearance of the style-transferred vector data, decomposing the translation into a sequence of intermediate steps that approximate a Schrödinger Bridge. Rather than relying on cyclic reconstruction to maintain structural alignment, UNSB achieves semantic consistency through gradual transport, distribution matching at each step, and explicit regularisation. This leads to a smoother and more controlled transformation from cartographic style and data-depended uncertainty of the original historical maps to style-transferred vector data and helps avoid the abrupt or unstable shifts that can occur in CycleGAN-based mappings, which is the rational behind our early-stopping strategy when training CycleGAN.

#### 4.3 Domain-adaptive semantic segmentation

To assess the realism of the synthetic maps and their effectiveness in the context of domain-adaptive semantic segmentation, we employ two evaluation strategies. (a) We compute the **Fréchet Inception Distance (FID)** to quantitatively measure the similarity between the synthetic and original maps. (b) We train **Self-Constructing Graph Convolutional Networks (SCGCN)** for land-cover classification and evaluate their performance on 125 manually annotated samples from the original homogeneous corpus, which the synthetic maps aim to replicate.

The SCGCN employed in this work was originally introduced by Liu et al. [36] and has demonstrated strong performance in various semantic segmentation tasks, including urban scene segmentation in remote sensing imagery [37], two-branch segmentation of indoor floorplans [38], and most importantly in the segmentation of heterogeneous historical map corpora [5]. For the semantic segmentation of a respective input map, each pixel needs to be assigned to one of the five land-cover classes  $C = \{\text{building, infrastructure, recreational surfaces, water bodies, sealed surfaces}\}$ . The SCGCN employed in this work was originally introduced by Liu et al. [36] and has demonstrated strong performance in various semantic segmentation tasks, including urban scene segmentation in remote sensing imagery [37], two-branch segmentation of indoor floorplans [38], and the segmentation of heterogeneous historical map corpora [5]. The

key advantage of this architecture lies in its ability to capture long-range dependencies within an image beyond local neighborhoods, without requiring an excessively deep network, by leveraging graph convolutional layers. The graph structure itself is learned automatically, eliminating the need for domain-specific expert knowledge. An overview of the SCGCN architecture is shown in Figure 6. The network consists

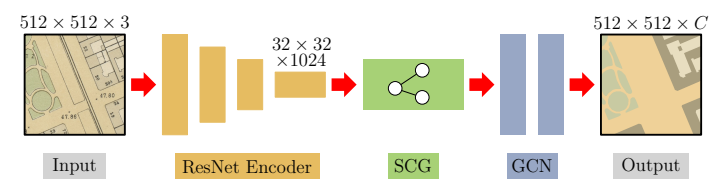


**Fig. 6**: Architecture of the underlying Self-Constructing Graph Convolutional Network (SCGCN).

of three parts. First, the input image is fed into a pretrained ResNet Encoder, in our case we use three layers of a ResNet-50. Second, the resulting features are used in the Self-constructing graph module (SCG), which forms the core of the network. Here, a graph structure is automatically induced, in which the features directly form the nodes. In addition, edges between two features are added based on their respective similarity. For this process, a new embedding for the features is learned based on Gaussian parameters  $\mu$  and  $\sigma$ . The latent variables are regularized by calculating the Kullback-Leibler divergence between a centered isotropic Gaussian prior distribution over the parameters and the new embedding. By essentially performing a similarity check between each pair of embeddings, edges are added between similar features. Third, the resulting graph is then fed into two graph convolutional layers, in the figure noted as GCN, which assign each pixel of the input image to one of the classes C. To overcome the well-known problems associated with imbalance classes in a dataset, Liu et al. [36] introduced the Adaptive Class Weighting Loss (ACW loss) which we applied in our work as well. For this, weights for the respective classes are computed by performing an iterative batch-wise class rectification instead of, using a fixed weight based on the frequency of occurrence in the whole dataset.

## 5 Experimental Results

To create a seamless mosaic of segmentation results, the Straube maps were manually georeferenced. For the sake of reproducibility and to support future benchmarking, the manually annotated test dataset for the Straube maps is publicly available at <a href="https://zenodo.org/records/17579452">https://zenodo.org/records/17579452</a>. The spatial consistency between adjacent image patches, which were processed independently during semantic segmentation, is crucial, as the segmented patches are reassembled into a seamless mosaic to reconstruct the full geographic extent of the original Straube map, supporting further analysis of the land-cover classes. For the sake of illustrating our bootstrapped training datasets, the semantic segmentation results and the full geographic extent of the original Straube maps, we developed a front end visualization hosted as a website at

### http://88.198.55.211/map/.

Implementation details. All experiments, including the generation of synthetic training data using CycleGAN and UNSB, as well as domain-adaptive semantic segmentation on the generated historical maps with the adapted SCGCN, were performed using GPU acceleration via CUDA. The experiments were conducted in PvTorch 2.2.0 with CUDA 12.8 on an NVIDIA RTX 2000 Ada GPU equipped with 8 GB VRAM. Each bootstrapped training dataset comprised 2,269 image pairs, each containing a historical map and its corresponding annotated ground truth. For CycleGAN, we employed the official PyTorch implementation provided by Zhu et al. [33], setting the learning rate for both the generator and discriminator to 0.0002, with a batch size of 1. For UNSB, we used the original PyTorch implementation from Kim et al. [34], also with a batch size of 1, and added Gaussian noise to the input data with a standard deviation of 0.15. For training the SCGCN, each dataset was randomly split into 80% training and 20% validation subsets. Importantly, the same random split was applied across both datasets to ensure fair and directly comparable results between models trained on different data variants. The SCGCN was trained using  $32 \times 32$  nodes in the Self-Constructing Graph module, while inference was performed with  $64 \times 64$  nodes. A batch size of 9 and a learning rate of  $3.47 \times 10^{-4}$  were used for all training runs.

FID. The FID is a widely used metric for evaluating the quality of images generated with generative models by quantifying their similarity to real images [35]. It measures the distance between two multivariate Gaussian distributions, representing the feature embeddings of real and generated images, using the Fréchet distance [39]. In our work, we use the FID to perform an unpaired image-to-image comparison between the generated maps and the original Straube maps. Each distribution is parameterized by its mean  $\mu$  and covariance matrix  $\Sigma$ , computed after transforming both sets of images from pixel space into a high-level feature space using the final pooling layer of an Inception-v3 network, as illustrated in Figure 7 [40]. The FID is then computed, incorporating the trace Tr of the covariance matrices, as shown in Equation 1. This enables the FID to capture perceptual differences based on semantic content rather than low-level pixel differences. Lower FID scores indicate greater similarity and therefore higher visual fidelity, while higher scores suggest larger discrepancies between the synthetic and real maps.

$$FID = \|\mu_X - \mu_Y\|^2 - Tr(\Sigma_X + \Sigma_Y - 2\sqrt{\Sigma_X \Sigma_Y})$$
 (1)

The FID results shown in Table 1 indicate that the training dataset degraded by

**Table 1**: FID scores for bootstrapped training datasets ↓.

dataset	style-transferred	st. degraded	$\mathrm{DL}_{\mathrm{CycleGAN}}$	$\mathrm{DL}_{\mathrm{UNSB}}$
Straube map	100.73	56.24	85.61 (Epoch 2)	<b>44.54</b> (Epoch 400)

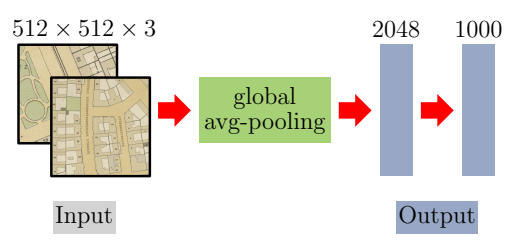
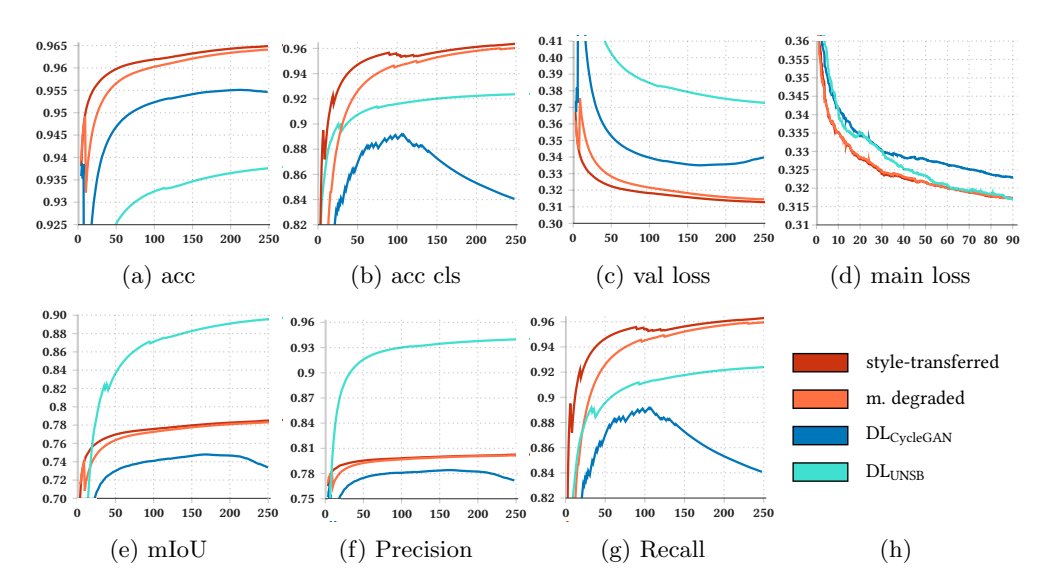


Fig. 7: Architecture illustrating the transformation into a high-level feature space based on the final layer of the Inception-v3 network.

UNSB exhibits the highest similarity to the original map corpora. Interestingly, the purely style-transferred dataset shows the lowest similarity to the original map corpora compared to the stochastically degraded dataset or the datasets degraded by CycleGAN. We interpret this observation as preliminary evidence that the datasets with explicit simulation of data-dependent uncertainty are likely to achieve superior performance in semantic segmentation of the original map corpora, owing to the high similarity of their latent feature representations extracted from the final layer of the Inception-v3 network.

## 5.1 Ablation Study



**Fig. 8**: Smoothed accuracy and loss curves during training (a-d) and validation metrics (e-g). The y-axis indicates the metric values, while the x-axis represents the number of epochs. For the main loss plot (d), the x-axis represents the number of training iterations, expressed in thousands.

In the following, we evaluate and discuss the performance of the synthetically bootstrapped training datasets on a homogeneous map corpus, namely the previously introduced Straube maps. To facilitate this evaluation and to individually assess the effectiveness of each training dataset, as mentioned, we manually annotated 125 Straube map patches, each of size  $500\times500$  pixels, using the same five land-cover classes employed in generating the training annotations, as detailed in Section 3. This ground truth dataset enables a robust evaluation of domain-adaptive learn-

**Table 2**: Overall per-dataset percentage values of accuracy, Kappa coefficient and  $F_1$  score using the SCGCN after [5] trained with bootstrapped datasets, evaluated on manually annotated test dataset.

metric	style-transferred	stochastically degraded	$\mathrm{DL}_{\mathrm{CycleGAN}}$	$\mathrm{DL}_{\mathrm{UNSB}}$
Accuracy	0.8357	0.8125	0.8716	0.8542
Kappa	0.7796	0.7499	0.8268	0.8024
$F_1$ score	0.8732	0.8623	0.9003	0.8464

ing and model inference performance on original historical maps. To ensure a fair and consistent comparison across all datasets, we used the same set of hyperparameters for training the SCGCN for experiment. The experimental outcomes are assessed using quantitative metrics commonly used in machine learning tasks. As illustrated in Figure 8, the models demonstrate strong learning capabilities early in the training process, but with performance metrics only marginally improving over time. Due to the limited gains observed beyond this point, training was terminated after 250 epochs.

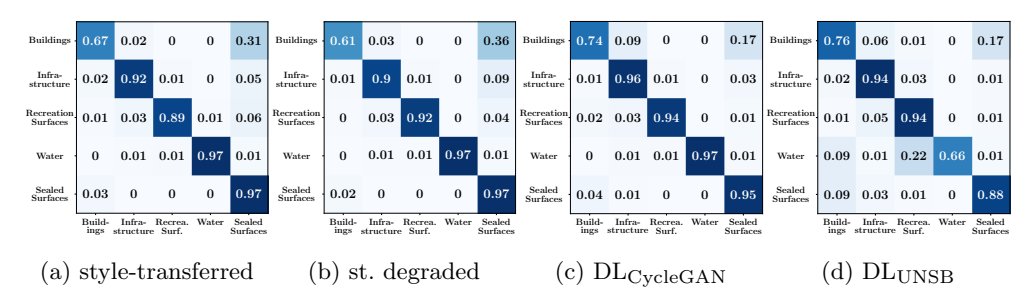


Fig. 9: Normalized confusion matrices. The Y-axis represents the true labels, while the X-axis shows the predicted labels.

As shown in Figure 8, the SCGCN models trained on the purely style-transferred dataset and stochastically degraded synthetic datasets exhibit similar trends across all evaluation metrics. Correspondingly, the validation and main loss curves also suggest a more stable and effective learning process for these models when compared to the models trained on automatically degraded synthetic datasets. Notably, the

DL<sub>CycleGAN</sub> dataset exhibits the weakest performance across nearly all metrics during training. Since only marginal performance improvements were observed beyond epoch 100, this epoch was selected for the semantic segmentation evaluation. Interestingly, evaluation of the model performance on the test dataset indicates that the DL<sub>CycleGAN</sub> dataset achieves the highest scores across all evaluation metrics, as presented in Table 3 and Table 2. With respect to accuracy and the Kappa coefficient, the model trained on the  $DL_{CycleGAN}$  dataset performs approximately 4% better than the style-transferred dataset, 6-7% better than the stochastically degraded dataset, and 2% better than the DL<sub>UNSB</sub> dataset. However, it is worth noting that although the DL<sub>CycleGAN</sub> dataset slightly outperforms the DL<sub>UNSB</sub> dataset, both automatically degraded datasets are competitive, with the GAN-based dataset showing a consistent but modest advantage. Based on this observation, we hypothesize that prolonged training on bootstrapped datasets can diminish the model's generalization capability to original historical maps. This limitation is likely attributable to overfitting on the synthetic training distribution, especially when the bootstrapped datasets exhibit insufficient realism and variation in simulated data-dependent uncertainty. An analysis of the normalized confusion matrices in Figure 9 indicates that, across all datasets, the highest rate of misclassification occurs in the buildings land-cover class, which is most frequently confused with the sealed surface class. The only exception is the model trained on the DL<sub>UNSB</sub> dataset, where the highest misclassification rate is observed in the water class, predominantly confused with recreational surfaces. Notably, the model with the highest metric scores overall trained on the DL<sub>CycleGAN</sub> dataset misclassifies buildings as infrastructure (approximately 9%), it more frequently confuses them with infrastructure (17%). This observation is further supported by the fact that the same model appears to visually perform best in accurately identifying infrastructure elements, such as streets, as can be identified in Figure 10.

Interestingly, the IoU and  $F_1$  scores for the land-cover classes buildings, recreational surfaces, and sealed surfaces are highest for the model trained on the  $DL_{CycleGAN}$  dataset, as shown in Table 3, a pattern that is also evident in the qualitative results in Figure 10. This finding is noteworthy because the individual recall and precision values for these classes are slightly lower than those of the respective best-performing models, except for the precision of sealed surfaces, where the the model trained on the  $DL_{CycleGAN}$  dataset marginally outperforms all others. Although the model trained on the  $DL_{CycleGAN}$  dataset achieves the highest accuracy (Figure 9c) and recall (Table 3) for the infrastructure class, it exhibits a markedly lower IoU (-5%) and  $F_1$  score (-3%) compared to the best-performing model in this case, which is the purely style-transferred dataset. This discrepancy suggests that the model may be overly liberal in predicting infrastructure, potentially leading to over-segmentation. Given that infrastructure often lies adjacent to both buildings and sealed surfaces, this could explain the reduced precision and overall performance for this class.

Visually, the datasets with automatic degradation used for semantic segmentation produce results with higher visual fidelity which is also supported by the quantitative evaluation on the test dataset. This may be due to the observation that deep generative approaches introducing excessive data-dependent uncertainty, also present

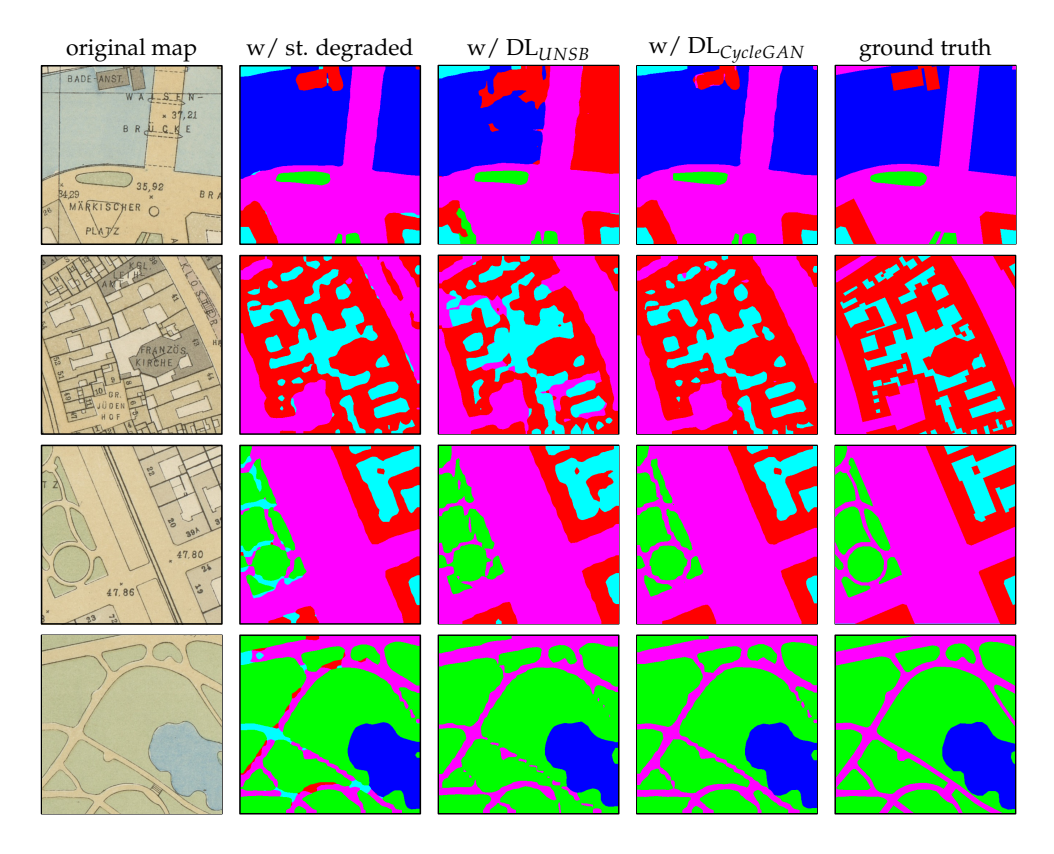


Fig. 10: Exemplary qualitative results of the domain-adaptive semantic segmentation using all bootstrapped datasets with simulated data-dependent uncertainty.

in the test dataset. Although often imperceptible to the human eye, this noise can positively impact the semantic segmentation model's performance, ultimately leading to improved accuracy. It is noteworthy that the results achieved with UNSB are not necessarily governed by explicit semantic layout reconstruction, in contrast to the other dataset generation approaches. This can be attributed to the way Stable Diffusion models operate with respect to the noise-denoise process, which is critical for image generation [34]. Nevertheless the maps generated by UNSB are promising and could potentially be further improved.

## 6 Conclusion & Future Work

Developing an approach capable of automatically generating *unlimited* quantities of annotated historical maps represents a crucial step toward the comprehensive digitization and interpretation of historical cartographic sources. This is particularly important because most state-of-the-art supervised methods for automatic map interpretation rely on deep learning, which inherently demands large volumes of annotated

**Table 3**: Per-class and overall per-dataset percentage values of Precision, Recall, IoU and  $F_1$  score using the SCGCN after [5] trained with bootstrapped datasets, evaluated on manually annotated test dataset.

	class	Precision	Recall	IoU	F <sub>1</sub> score
style-transferred	Buildings	0.9578	0.6697	0.6506	0.7883
	Infrastructure	0.9437	0.9224	0.8743	0.9329
	Recr. surfaces	0.9754	0.8913	0.8718	0.9315
	Water bodies	0.9553	0.9660	0.9243	0.9606
	Sealed surfaces	0.6152	0.9692	0.6034	0.7527
	Overall	0.7412	0.7364	0.6540	0.8732
st. degraded	Buildings	0.9653	0.6109	0.5978	0.7483
	Infrastructure	0.9340	0.8955	0.8423	0.9144
	Recr. surfaces	0.9788	0.9228	0.9047	0.9500
	Water bodies	0.9777	0.9718	0.9507	0.9747
	Sealed surfaces	0.5762	0.9743	0.5676	0.7242
	Overall	0.7387	0.7292	0.6438	0.8623
DLCycleGAN	Buildings	0.9555	0.7361	0.7117	0.8316
	Infrastructure	0.8604	0.9583	0.8295	0.9068
	Recr. surfaces	0.9682	0.9354	0.9075	0.9515
	Water bodies	0.9748	0.9732	0.9494	0.9740
	Sealed surfaces	0.7477	0.9520	0.7205	0.8375
	Overall	0.7511	0.7592	0.6864	0.9003
DLUNSB	Buildings	0.9107	0.7613	0.7085	0.8293
	Infrastructure	0.8739	0.9439	0.8309	0.9076
	Recr. surfaces	0.8823	0.9362	0.8323	0.9085
	Water bodies	0.9659	0.6555	0.6407	0.7810
	Sealed surfaces	0.7460	0.8755	0.6744	0.8056
	Overall	0.7298	0.6954	0.6145	0.8464

training data. In this work, we introduced an automated framework that transfers the cartographic style of specific historical map corpora onto contemporary geospatial vector data, such as OpenStreetMap (OSM). To enhance the realism and domain fidelity of the synthesized data, our approach automatically applies corpus-specific degradations that simulate data-dependent uncertainties, including noise originating material deterioration and scanning artifacts. We assessed the effectiveness of the proposed framework through a comprehensive evaluation using a deep learning-based semantic segmentation model trained exclusively on the generated synthetic maps. The results demonstrate that domain-adaptive semantic segmentation trained solely on synthetically bootstrapped data can achieve an accuracy of approximately 88% when applied to original historical maps, underscoring the potential of our method for large-scale, automated map interpretation. Future work will focus on improving

the geometric and semantic consistency of the generated maps by incorporating automatic mechanisms that explicitly enforce spatial coherence and simulate uncertainty in a more principled manner. One possible direction for future work is the adoption of loss functions designed to enforce geometric consistency during generation, thereby enabling GAN models to be trained over longer epochs without loss of semantic consistency and spatial coherence. Another promising avenue involves integrating the proposed framework with advanced diffusion-based generative models, such as Stable Diffusion (SD), in combination with ControlNet [23] to further enhance style transfer by constraining the generation process through explicit semantic layout conditioning. Ultimately, this combination could eliminate the need for manual style transfer and fully automate the generation of high-fidelity, semantically aligned synthetic historical maps.

Although Wu et al. [4] argue that increasing the amount of training data alone cannot resolve data-dependent uncertainty, our results demonstrate that simulating such uncertainties within synthetically generated training data can lead to highly successful deep learning-based semantic segmentation of homogeneous historical map corpora even in the absence of any real ground truth data. By reducing the time required to generate annotated training data to just a few hours, our approach significantly lowers the cost and effort involved.

This work represents an important milestone toward unlocking the vast potential of digitized historical map archives. By enabling the automatic and scalable generation of annotated cartographic data, our approach paves the way for the large-scale interpretation of thousands of scanned historical maps, revealing spatial, cultural, and environmental information that has remained inaccessible to computational analysis for centuries.

# Acknowledgements

We gratefully acknowledge the Staatsbibliothek zu Berlin for providing access to the *Julius Straube* map collection. We further extend our thanks to Jannik Matijevice for his assistance in annotating the test data employed for evaluation and Lena Hildebrandt for developing the web viewer used to visualize the generated datasets and segmentation results.

#### References

- [1] Chiang, Y.-Y., Duan, W., Leyk, S., Uhl, J.H., Knoblock, C.A.: Using Historical Maps in Scientific Studies: Applications, Challenges, and Best Practices, (2020). https://doi.org/10.1007/978-3-319-66908-3
- [2] Li, Z., Guan, R., Yu, Q., Chiang, Y.-Y., Knoblock, C.A.: Synthetic map generation to provide unlimited training data for historical map text detection. In: Proceedings of the 4th ACM SIGSPATIAL International Workshop on AI for

- Geographic Knowledge Discovery. GEOAI '21, pp. 17–26. Association for Computing Machinery, New York, NY, USA (2021). https://doi.org/10.1145/3486635. 3491070
- [3] Wu, S., Heitzler, M., Hurni, L.: Leveraging uncertainty estimation and spatial pyramid pooling for extracting hydrological features from scanned historical topographic maps. GIScience & Remote Sensing **59**(1), 200–214 (2022) https://doi.org/10.1080/15481603.2021.2023840
- [4] Wu, S., Chen, Y., Schindler, K., Hurni, L.: Cross-attention spatio-temporal context transformer for semantic segmentation of historical maps. In: Proceedings of the 31st ACM International Conference on Advances in Geographic Information Systems. SIGSPATIAL '23. Association for Computing Machinery, New York, NY, USA (2023). https://doi.org/10.1145/3589132.3625572
- [5] Arzoumanidis, L., Knechtel, J., Haunert, J.-H., Dehbi, Y.: Semantic segmentation of historical maps using self-constructing graph convolutional networks. Cartography and Geographic Information Science (2025) https://doi.org/10.1080/ 15230406.2025.2468304
- [6] Uhl, J.H., Leyk, S., Chiang, Y.-Y., Knoblock, C.A.: Towards the automated large-scale reconstruction of past road networks from historical maps. Computers, Environment and Urban Systems 94, 101794 (2022) https://doi.org/10.1016/ j.compenvurbsys.2022.101794
- [7] Sertel, E., Hucko, C.M., Kabadayı, M.E.: Automatic road extraction from historical maps using transformer-based segformers. ISPRS International Journal of Geo-Information 13(12) (2024) https://doi.org/10.3390/ijgi13120464
- [8] Jiao, C., Heitzler, M., Hurni, L.: A novel framework for road vectorization and classification from historical maps based on deep learning and symbol painting. Computers, Environment and Urban Systems 108, 102060 (2024) https://doi. org/10.1016/j.compenvurbsys.2023.102060
- [9] Uhl, J.H., Leyk, S., Li, Z., Duan, W., Shbita, B., Chiang, Y.-Y., Knoblock, C.A.: Combining remote-sensing-derived data and historical maps for long-term backcasting of urban extents. Remote Sensing 13(18) (2021) https://doi.org/10.3390/ rs13183672
- [10] López-Rauhut, M., Zhou, H., Aubry, M., Landrieu, L.: Segmenting france across four centuries. In: Yin, X.-C., Karatzas, D., Lopresti, D. (eds.) Document Analysis and Recognition – ICDAR 2025, pp. 3–22. Springer, Cham (2026). https://doi. org/10.1007/978-3-032-04617-8\_1
- [11] Mäyrä, J., Kivinen, S., Keski-Saari, S., Poikolainen, L., Kumpula, T.: Utilizing historical maps in identification of long-term land use and land cover changes. Ambio 52(11), 1777–1792 (2023) https://doi.org/10.1007/s13280-023-01838-z

- [12] Arzoumanidis, L., Fethers, J.O., Mudiyanselage, S.H., Dehbi, Y.: Deep generation of synthetic training data for the automated extraction of semantic knowledge from historical maps. Abstracts of the ICA 7, 7 (2024) https://doi.org/10.5194/ica-abs-7-7-2024
- [13] Wu, S., Schindler, K., Heitzler, M., Hurni, L.: Domain adaptation in segmenting historical maps: A weakly supervised approach through spatial co-occurrence. ISPRS Journal of Photogrammetry and Remote Sensing 197, 199–211 (2023) https://doi.org/10.1016/j.isprsjprs.2023.01.021
- [14] Xia, X., Balestriero, R., Zhang, T., Zhou, Y., Ding, A., Saini, D., Hurni, L.: Map-SAM2: Adapting SAM2 for Automatic Segmentation of Historical Map Images and Time Series (2025). https://arxiv.org/abs/2510.27547
- [15] Sterzinger, R., Peer, M., Sablatnig, R.: Few-Shot Segmentation of Historical Maps via Linear Probing of Vision Foundation Models (2025). https://arxiv.org/abs/2506.21826
- [16] Yuan, Y., Sester, M.: Leveraging LLMs and attention-mechanism for automatic annotation of historical maps (2025). https://doi.org/10.48550/arXiv.2504.11050
- [17] Duan, W., Chiang, Y., Chen, T., Gerlek, M.P., Jang, L., Kirsanova, S., Knoblock, C.A., Lin, F., Lin, Y., Li, Z., Minton, S.N.: Digmapper: A modular system for automated geologic map digitization. In: Proceedings of the ACM SIGSPATIAL International Conference on Advances in Geographic Information Systems (SIGSPATIAL '25), Minneapolis, MN (2025)
- [18] Bird, J.J., Lotfi, A.: Cifake: Image classification and explainable identification of ai-generated synthetic images. IEEE Access 12, 15642–15650 (2024) https://doi.org/10.1109/ACCESS.2024.3356122
- [19] Kloukiniotis, A., Papandreou, A., Anagnostopoulos, C., Lalos, A., Kapsalas, P., Nguyen, D.-V., Moustakas, K.: Carlascenes: A synthetic dataset for odometry in autonomous driving. In: Proceedings of the IEEE/CVF Conference on Computer Vision and Pattern Recognition (CVPR) Workshops, pp. 4520–4528 (2022). https://doi.org/10.1109/CVPRW56347.2022.00498
- [20] Kirsanova, S., Chiang, Y.-Y., Duan, W.: Detecting Legend Items on Historical Maps Using GPT-40 with In-Context Learning (2025)
- [21] Mühlematter, D.J., Schweizer, S., Jiao, C., Xia, X., Heitzler, M., Hurni, L.: Probabilistic road classification in historical maps using synthetic data and deep learning (2024). https://arxiv.org/abs/2410.02250
- [22] Affolter, C., Wu, S., Chen, Y., Hurni, L.: Generative AI in Map-Making: A Technical Exploration and Its Implications for Cartographers. arXiv (2025). https://doi.org/10.48550/ARXIV.2508.18959

- [23] Zhang, L., Rao, A., Agrawala, M.: Adding conditional control to text-to-image diffusion models. In: Proceedings of the IEEE/CVF International Conference on Computer Vision (ICCV), pp. 3836–3847 (2023)
- [24] Arzoumanidis, L., Hecht, J., Dehbi, Y.: Towards a deep automatic generation of figure-ground maps. ISPRS Annals of the Photogrammetry, Remote Sensing and Spatial Information Sciences **X-4/W5-2024**, 33–39 (2024) https://doi.org/10.5194/isprs-annals-X-4-W5-2024-33-2024
- [25] Yuan, Y., Thiemann, F., Dahms, T., Sester, M.: Semantic segmentation of time-series of historical maps by learning from only one map. International Journal of Cartography, 1–15 (2025) https://doi.org/10.1080/23729333.2025.2545586
- [26] Xia, X., Zhang, D., Song, W., Huang, W., and, L.H.: MapSAM: adapting segment anything model for automated feature detection in historical maps. GIScience & Remote Sensing 62(1) (2025) https://doi.org/10.1080/15481603.2025.2494883
- [27] Yuan, Y., Thiemann, F., Dahms, T., Sester, M.: SMOL-MapSeg: Show Me One Label (2025). https://arxiv.org/abs/2508.05501
- [28] Wang, C., Kang, Y., Gong, Z., Zhao, P., Feng, Y., Zhang, W., and, G.L.: Cartoagent: a multimodal large language model-powered multi-agent cartographic framework for map style transfer and evaluation. International Journal of Geographical Information Science, 1–34 (2025) https://doi.org/10.1080/13658816. 2025.2507844
- [29] OpenStreetMap contributors: OpenStreetMap: Collaborative Project to Create a Free Editable Map of the World. https://www.openstreetmap.org. Accessed: October 25, 2025 (2025)
- [30] MapTiler: MapTiler Maps for developers. https://www.maptiler.com/. Accessed: 2025-11-14 (2025)
- [31] Maputnik: Maputnik Open-source visual editor for the MapLibre Style Specification. https://maputnik.github.io/. Accessed: 2025-11-14 (2025)
- [32] Wu, S., Heitzler, M., Hurni, L.: A closer look at segmentation uncertainty of scanned historical maps. The International Archives of the Photogrammetry, Remote Sensing and Spatial Information Sciences XLIII-B4-2022, 189–194 (2022) https://doi.org/10.5194/isprs-archives-XLIII-B4-2022-189-2022
- [33] Zhu, J.-Y., Park, T., Isola, P., Efros, A.A.: Unpaired image-to-image translation using cycle-consistent adversarial networks. In: 2017 IEEE International Conference on Computer Vision (ICCV), pp. 2242–2251 (2017). https://doi.org/10. 1109/ICCV.2017.244
- [34] Kim, B., Kwon, G., Kim, K., Ye, J.C.: Unpaired image-to-image translation via

- neural schrödinger bridge. In: ICLR (2024)
- [35] Heusel, M., Ramsauer, H., Unterthiner, T., Nessler, B., Hochreiter, S.: Gans trained by a two time-scale update rule converge to a local nash equilibrium. In: Proceedings of the 31st International Conference on Neural Information Processing Systems. NIPS'17, pp. 6629–6640 (2017)
- [36] Liu, Q., Kampffmeyer, M., Jenssen, R., Salberg, A.-B.: Multi-view self-constructing graph convolutional networks with adaptive class weighting loss for semantic segmentation. In: Proceedings of the 2020 IEEE/CVF Conference on Computer Vision and Pattern Recognition Workshops (CVPRW 2020), pp. 199–205 (2020). https://doi.org/10.1109/CVPRW50498.2020.00030
- [37] Liu, Q., Kampffmeyer, M., Jenssen, R., Salberg, A.-B.: Self-constructing graph neural networks to model long-range pixel dependencies for semantic segmentation of remote sensing images. International Journal of Remote Sensing 42(16), 6184–6208 (2021) https://doi.org/10.1080/01431161.2021.1936267
- [38] Knechtel, J., Rottmann, P., Haunert, J.-H., Dehbi, Y.: Semantic floorplan segmentation using self-constructing graph networks. Automation in Construction 166, 105649 (2024) https://doi.org/10.1016/j.autcon.2024.105649
- [39] Har-Peled, S., Raichel, B.: The fréchet distance revisited and extended. ACM Trans. Algorithms **10**(1) (2014) https://doi.org/10.1145/2532646
- [40] Szegedy, C., Vanhoucke, V., Ioffe, S., Shlens, J., Wojna, Z.: Rethinking the inception architecture for computer vision. In: Proceedings of the IEEE Conference on Computer Vision and Pattern Recognition (CVPR) (2016)